OEA | Opto-Electronic Advances

Article

July 2026, Vol. 9, No. 7

Open Access

A flexible wireless system for prospective photodynamic therapy applications

Rolan Mansour[1]*, Bhavani Yalagala[1], Vikas Vikas[4], Nikolas Bruce[1], Fawziye Tarhini[1], Georgios N. Arvanitakis[2], Mohammed Mughal[1], Jamie Blanche[1], Ahmad Taha[1], Jonathan Copper[5], Muhammad Imran[1], Karin Williams[3], Karin Oien[3], Mahmoud Wagih[1], Hadi Heidari[1], Robert Hadfield[4] and David Flynn[1]

Abstract: Cancer treatments, dependent on several factors, deliver varying degrees of treatment effectiveness. Photodynamic therapy (PDT) is a treatment modality that selectively targets and destroys cancer cells using a light-sensitive drug with a specific optical wavelength. However, PDT encounters several constraints, mainly, limited penetration of light into deep tumors. In this paper, we present a new wireless implantable PDT system towards overcoming the constraints of current PDT treatments. The wireless-powered prototype was evaluated showing resonant inductive power delivery in a tissue phantom, emulating the bladder, providing the necessary power level for PDT treatment. The production of singlet oxygen ($^1O_2$) using a multi-LED system was studied by utilizing a 1,3-diphenylisobenzofuran (DPBF) in a Rose Bengal (RB) and Dimethyl sulfoxide (DMSO) solution, under both DC and AC excitations, for direct wireless powering. The photosensitizer solution is illuminated with over 5 mW of optical power generated by the four-LED array to generate $^1O_2$. Our measurements confirm the production of $^1O_2$ emissions as well as lifetime performance. The optical, electrical, and mechanical studies are presented on the resultant optoelectronic system, verifying the efficiency and mechanical robustness of our prototype. A fabrication flow for biocompatible devices using laser ablation is also introduced towards large area manufacturability, scalability, and repeatability. Our manufacturing process is versatile to a variety of materials including polymeric substrates, metallic electrodes and offers design flexibility ranging from 30 microns to mm. This research advances the development of wirelessly powered implantable device for PDT, optimized for *in-vivo* use through careful LED selection and biocompatible design. Our results evidence the potential of a new emergent technology that addresses the limitations of PDT as a potential future therapy to enhance the curative efficiency of cancer treatment and demonstrates promising preliminary potential for in vivo application, which requires further validation before therapeutic implementation can be established.

Keywords: photodynamic therapy; bladder cancer; urothelial carcinoma; microsystem; parylene C; flexible; implantable; wireless and biomedical device; photosensitizers; micro-LED; singlet oxygen

DOI: 10.29026/oea.2026.250275 | CSTR: 32247.14.oea.2026.250275

Citation: Mansour R, Yalagala B, Vikas V et al. A flexible wireless system for prospective photodynamic therapy applications. *Opto-Electron Adv* **9**, 250275 (2026).

1 Introduction

Every year, millions of people are diagnosed with cancer, a disease that poses a significantly growing global health concern[1]. In 2020, 10 million people died from cancer worldwide, and this figure has been rising for decades[2]. Nevertheless, in many instances, cancer is potentially curable if it is diagnosed and treated early, before metastatic spread or invasion into adjacent organs. In the developed nations, one in three people is expected to develop a form of cancer during their lifetime[3]. The elevated rate of cancer in such countries can be linked to numerous factors, including

Received: 13 October 2025

Accepted: 14 April 2026

Published online: 15 May 2026

[1]James Watt School of Engineering, University of Glasgow, Glasgow G12 8QQ, UK; [2]Edinburgh Instruments Ltd, 2 Bain Square, Kirkton Campus, Livingston EH54 7DQ, UK; [3]School of Cancer Sciences, University of Glasgow, Glasgow G61 1QH, UK; [4]Quantum Sensors Group, Advanced Research Centre, University of Glasgow, Glasgow G11 6EW, UK; [5]Biomedical Engineering, Advanced Research Centre, University of Glasgow, Glasgow G12 8QQ, UK.
*Correspondence: R Mansour, E-mail: rolan.mansour@glasgow.ac.uk

longer life expectancies, enhanced diagnostic skills, and the prevalence of lifestyle-related risk factors such as poor diet, smoking, and lack of physical activity[4]. Conventional cancer management relies primarily on surgery alone or in combination with chemotherapy and/or radiation. Newer modalities such as targeted chemotherapy and immunotherapy expand the toolbox available for the treatment of carcinomas[5]. Regardless of how effective the cancer treatments are, they can have unintended consequences and aftereffects[6] caused by non-specific targeting of normal cells, dysregulated immune cells, and the induction of systemic and local toxicity during treatment[7]. Cancer cells that evade these therapies lead to recurrence and the generation of treatment-resistant clonal populations[7]. Accordingly, therapeutic strategies are determined by the type, location, and stage of the carcinoma, as well as the patient's general health and preferences, all of which influence the clinical management of the patient[8].

Bladder cancer accounts for approximately 3% of the total cancer cases globally and is considered the most diagnosed with cancer worldwide. The World Health Organization ranked bladder cancer as the ninth most common type of cancer and the thirteenth cause of cancer-related deaths worldwide. The incidence of bladder cancer shows a marked sex disparity, with higher incidence in men compared to that in women (1 in 27 men vs. 1 in 89 women). Urothelial cancer is the most common type of bladder cancer accounting for 90% of cases. Squamous cell carcinoma and adenocarcinoma make up 5% and 2%, respectively, correlating with advanced stages and higher mortality compared to urothelial carcinoma[9]. Bladder cancer can also be further characterized as either muscle invasive (MIBC) or non-muscle invasive (NMIBC), both of which have their own molecular signatures and microenvironments, however as expected pMIBC is the more aggressive of the two types[10].

Treatments for bladder cancers are largely based on the trilogy of surgery, chemotherapy and radiation, and combinations thereof. When treating bladder cancer, the most common standard treatment approach typically involves the removal of neoplastic fragments[11]. Unfortunately, more than 70% of patients experience a relapse following their initial treatment. Additional treatment modalities include chemotherapy and intravesical immunotherapy, which are generally recommended for patients at a higher risk of recurrence. While intravesical chemotherapy can reduce the tumor burden in the short term, it does not always alter the cancer progression. Bladder cancer exhibits a diverse natural course, with some tumors being classified as low-grade. These tend to progress slowly, often requiring initial treatment through endoscopy and ongoing monitoring, but they usually present a minimal threat to the patient's health[12]. Scientific research efforts focus on developing more effective, less invasive, cost-effective cancer treatments, with a focus on minimizing the harm caused to normal healthy cells. One such promising treatment is photodynamic therapy (PDT). PDT targets and kills cancer cells by combining light-absorbing chemicals (photosensitizers) that specifically accumulate in malignant cells with light of specific wavelength in presence of oxygen[13]. Upon absorbing the light, the photosensitizers undergo a photochemical reaction. These reactions catalyze an altered biochemical state within cells, i.e., causing a biochemical chain reaction resulting in cell death. PDT is well established as a treatment for basal cell carcinoma and squamous cell carcinoma of the skin[14], but its potential to treat other cancers is mainly restricted to preclinical or early clinical trials. Skin cancers lead the way in PDT therapy as the skin is uniquely easily exposed to light, while most carcinomas are deep within the body. However, with innovative engineering, these sites can be accessed to deliver light to the tumour site and the development of more effective, novel photosensitizers tailored to the cancer will increase the scope of PDT as a treatment modality.

Over the years, numerous effective treatment modalities have been developed for bladder cancer, including PDT, as well as new drugs that aimed at managing the disease's effects[15]. The bladder is an excellent candidate for PDT; it is readily accessible and is readily exposed to chemotherapy agents. Because bladder cancer can be localized, thin and superficial if diagnosed at early stages, this makes PDT a novel treatment approach that can be effective compared to other treatment modalities. Recently, PDT was frequently used in clinical practices to treat superficial bladder cancer, it exploits the differential uptake of PS localized light penetration to the bladder using cystoscopy, to induce oxidative damage targeting directly the tumour lesion and causing vascular shutdown within tumor tissue, with minimal tissue damage to healthy surrounding tissue, providing a non-invasive, localized and pleasant treatment, and may further induce local immune responses against tumour cancer cells[16]. However, conventional PDT for bladder cancer treatment is constrained by the need for external light delivery, which is challenging due to the conformational changes the bladder undergoes due to organ movement, combined with the requirement for precise light dosimetry[17] making PDT a time-intensive therapy requiring repeated cystoscopic intervention.

There are more significant drawbacks to traditional PDT systems that use laser equipment with an endoscope or optical fibers. First, the applicability range of PDT is severely limited and depends strongly on tissue composition, wavelength, and optical power. While endoscopes and optical fibers primarily deliver light to the exposed epithelial layer, careful selection of wavelength and optimization of light intensity are required to achieve deeper tissue penetration, which is typically limited to the superficial layers in standard clinical settings[18]. Furthermore, a laser with high coherence and intensity causes a quick photodynamic reaction, which shortens the therapeutic effect[19]. The current laser-based PDT technique also has a problem with limited

treatment accessibility and portability because of the bulky and somewhat expensive laser equipment[20].

Wireless implanted PDT systems have lately been actively researched to overcome these restrictions[21,22]. Therefore, to overcome these limitations, a PDT micro-system has been developed, providing a more flexible and efficient approach to bladder cancer treatment. Because implantable PDT devices with wireless operation in the human body can be operated anytime, anyplace, and can also deliver light to deep-seated tumours, significantly extending the usable range of PDT, they offer enhanced accessibility and therapeutic impact. PDT can be combined with surgery, chemotherapy, or immunotherapy to increase its effectiveness[23,24]. Ongoing research utilizing LED devices in PDT has identified anti-tumour immunity induction resulting in total tumour shrinkage and prevention of tumour recurrence[25,26].

An implantable photonic strategy, which uses device stacking light emitting diode (LEDs), small-sized LEDs, or wireless LED systems, has emerged to increase the effectiveness and safety of PDT[27]. Because of the devices' tiny size, it is now possible to directly implant them into the centre of tumour tissues, effectively controlling and delivering the ideal amount of visible light deep within the tumours. Consequently, these implantable photonic devices have unique advantages: To activate photosensitizers, they can be implanted in tumour sites anywhere in the body, including deep within organs; (i) they enable multiwavelength light emission at a lower intensity; and (ii) they provide controlled light emission for accurate and precise light delivery at the ideal intensity of 10–150 mW/cm^2 depending on the type of application[18]. As a result, tumours can be effectively spatially and temporally treated using a programmable LED device.

Furthermore, the implantable photonic devices are ready to deliver therapeutic dosages of light in the tumour tissues inaccessible by direct lighting of an external light source. They stack several micro-scale LEDs to enable direct implantation into the target region. The device can be directly implanted into the inner core of tumour tissues, which enables light activation of photosensitizers throughout the entire tumour tissue. The micro-system is engineered to stack several LEDs in a parallel array rather than utilizing a single giant LED to reduce heat generation during micro-LED guided PDT[28].

From this perspective, a micro-LED that can be carefully inserted into tumours to efficiently supply light with finely adjusted intensity makes PDT attractive as a clinical management for carcinomas. In this work, we demonstrate that our approach to the fabrication of a flexible micro-LED capable of delivering PDT when combined with a photosensitizer, is both feasible and easily achievable. Such an approach of delivering modest visible light deep into tumors in thick biological tissue on demand should achieve biological control by direct killing of tumor cells and immune modulation of the environment[29].

Realizing such a system requires precise microscale engineering, which is where microfabrication plays a critical role. Microfabrication, which involves the design and creation of devices at the microscale, has revolutionized medical technology by enabling the development of highly precise, miniaturized medical devices capable of performing complex functions within the human body[30]. These systems offer several advantages, including minimal invasiveness[31] high precision[32,33] and the ability to integrate with other therapeutic modalities[34], making them ideal for applications in bladder cancer treatment[35]. However, most state-of-the-art optogenetic photodynamic therapy (PDT) devices rely on traditional cleanroom-based microfabrication approaches[36], which are costly, time-consuming, and require extensive exposure to toxic chemicals such as photoresists and developers. Such processing steps may adversely affect the biocompatibility of the resulting substrates[37]. In addition, these conventional techniques are often incompatible with polymeric and biopolymeric flexible materials that are desirable for implantable and biocompatible applications[38].

To address these limitations, alternative fabrication strategies such as soft lithography, spray coating, electrospinning, and advanced printing techniques, including inkjet printing, screen printing, and 3D printing, have been explored[39]. Although these methods enable rapid prototyping, scalability, and reduced material waste, they still face challenges related to precise patterning, resolution, and adhesion, particularly for emerging flexible and stretchable electronic devices[40]. Laser-based fabrication approaches offer a promising solution by providing enhanced material versatility, high-resolution patterning, scalability, and design flexibility. This approach may enable future translation toward clinical therapeutic applications, subject to further experimental and in vivo validation.

Optoelectronic systems play a critical role in PDT by delivering controlled light intensities required for photosensitizer activation[41]. Nevertheless, existing optoelectronic platforms continue to face limitations related to mechanical flexibility, biocompatibility, and heat dissipation[42]. The conventional microfabrication techniques such as photolithography, etching, and deposition are not only time consuming, costly but also need sophisticated equipment's for its operation[43]. Further, these methods not compatible with various upcoming flexible, biocompatible and biodegradable natural and synthetic polymers and use lots of chemicals during the processing which can hider the biocompatibility of the materials[44]. To address these challenges, we report a fully flexible, potentially biocompatible, low heat-dissipative, and implantable optoelectronic system fabricated using a high-resolution ultrafast laser ablation–based rapid prototyping approach. The device consists of an array of microscale light-emitting diodes (micro-LEDs) embedded on gold-patterned electrodes fabricated on a Parylene C substrate. The system incorporates four micro-LEDs capable of generating controlled light intensities suitable for PDT applications. Figure 1 presents a

schematic illustration of the multilayer optoelectronic module, comprising stacked layers of Parylene C, Ti/Au electrodes, micro-LEDs, and a top Parylene C encapsulation layer. A detailed description of the fabrication process is provided in the Section *Materials and Methods*.

In this work, we introduce a ground-breaking treatment modality in response to the unmet clinical need for bladder cancer through a novel PDT implantable medical system. The implantable, wireless-powered-LED-driven PDT that will use low levels of visible light to enhance antitumor immunity by activating photosensitizers deep within the bladder is presented in Fig. 1(a) and 1(b). The recommended laser-based microfabrication offers numerous advantages in terms of the material versatility, design flexibility, large area manufacturability and rapid fabrication. Moreover, the approach is very cost effective, generate less chemical waste and doesn't affect the properties of the materials especially biocompatibility and biodegradability. The electrical, optical, and mechanical characteristics of the proposed optoelectronic device are studied further in conjunction with *in-vitro* experiments to excite the photosensitive polymer. The optoelectronic system allows the precise placement of light sources directly within the bladder, facilitating uniform light distribution and reducing the invasiveness of continued treatments post-implantation due to its miniaturized (40 mm diameter) footprint. This approach can significantly improve patients' comfort as multiple endoscopies or surgeries for fiber optic insertion are avoided. Tumour targeting can increase the impact of PDT by protecting the normal bladder urothelium from nonspecific PS uptake and PDT damage[45]. The system demonstrates encouraging performance under the studied conditions, indicating potential therapeutic relevance.

2 Materials and methods

2.1 Materials and equipment

Parylene C dimer was purchased from Specialty Coating Systems (SCS) UK. Ultra-pure metals of Titanium and Gold were used, and all the metal depositions were done in the James Watt Nanofabrication Center (JWNC), a central facility based in University of Glasgow. Power Supply from RS components is used, and the manual probe station from Inseto is used for electrical measurements. Sheet resistance was measured using Ossila sheet resistance measurement instrument with a customized software associated with it. The output optical power of the LEDs was quantified using a Thorlabs (PM400) optical power meter.

Wireless power inductive coils were designed and simulated using Keysight Advanced Design Software. The current wireless power transfer (WPT) prototype device has been manufactured by JLC PCB on a commercial flexible polyimide substrate, with a polyimide coating. The production of singlet oxygen using an in-house developed LED system has been studied by utilizing a 1,3-diphenylisobenzofuran in a Rose Bengal (RB)and Dimethyl sulfoxide (DMSO) solution. This was analyzed using an FLS1000 photoluminescence spectrometer equipped with a standard cuvette holder (N-J01, Edinburgh Instruments).

2.2 Methods

2.2.1 Fabrication of flexible and implantable microelectrodes

Microelectrodes were designed and fabricated using gold electrodes (Ti/Au) on a fully flexible and biocompatible medical-grade Parylene C substrate and miniaturized micro-LEDs were interconnected with the electrodes. Various optimizations in terms of power, number of repetitions, and frequency were done to achieve precise fabrication of the proposed optoelectronic PDT system. A uniform Titanium/Gold Ti/Au (10/90 nm) was coated on the prepared Parylene C film using E-beam evaporation technique at a very slow deposition rate of 0.3/nm at ultra-high vacuum of 10^{-6} mbar. A shadow mask was prepared using the PET sheet. The Ti/Au-Parylene C substrate was used to

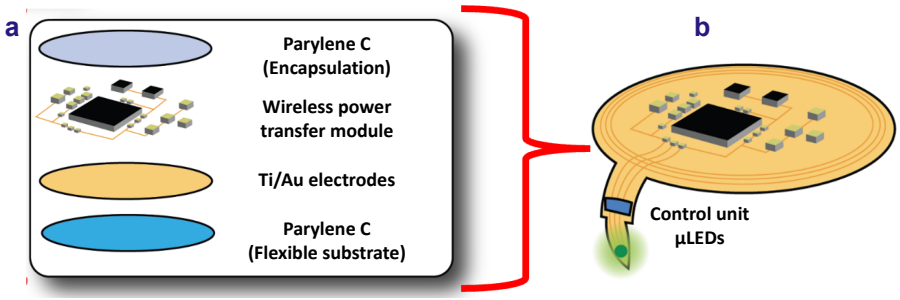


Fig. 1 | Schematic representation of the fully flexible, implantable and wirelessly powered optoelectronic system fabricated using advanced laser-based methodology for the treatment of the long-term cancer cells using PDT. (a) Optoelectronic system using gold electrodes on a Parylene C. (b) A high resolution-based ablation laser with an array of micro-scale LED device (micro-LEDs) embedded on the gold based patterned electrodes on Parylene C substrate with gold electrodes with an array of four LEDs generating a controlled light intensity was fabricated using rapid prototyping and ultra-fast ablation-based lasers.

evaluate the LEDs and the electro-optic. The Gerber files for the printed circuit board (PCB) were designed using Fusion 360 to create the geometry, and the .dxf file is generated which is further used for fabrication. An LPKF laser system (protomat) with ultraviolet (UV) light source of wavelength (λ=324 nm) was used as the etching tool to fabricate the flexible PDT system. Various optimizations such as number of repetitions, laser power, speed etc. were performed to achieve precise etch rate of the Ti/Au layer without any adverse effects to the substrate. The current vs voltage characteristics were recorded using the probe station to determine the line connectivity and sheet resistance measurements using the 4-point probe method were performed under flat and bent conditions. Similar experiments were performed on the Cu coated on Polyamide substrate with optimized parameters of laser power, speed, and number repetitions.

2.2.2 Preparation of flexible Parylene C films

The Parylene C was used as a flexible and biocompatible substrate and as an encapsulation layer using a SCS coating machine. Initially, a transparent 5 cm × 5 cm borosilicate glass substrate was cleaned using the isopropyl alcohol (IPA), Acetone, and DI water to remove any contaminants or other unwanted particles which may interfere with the substrate. Then the glass substrate is properly dried and have performed a UV-Ozone treatment for 60 seconds in a UV-Ozone machine from Ossila instruments. Next, the glass substrate is loaded on to the rotating substrate holder inside the chamber and ensure the substrate is positioned to prevent any further movements with a Kapton tape or double-sided tape. An already optimised quantity of 10 g of Parylene C was loaded into the vaporiser chamber of SCS coating machine to get a 7.5 μm thick film. Optimization of the Parylene C is already done and is tabulated from the manufacturer and is cross checked with the profilometer (Dektaideal) measurements. The chamber pressure was maintained at 15 mbar and the chiller is connected to the chamber and control the temperature of chamber to 690 °C to vaporise the powder. Switch on the vaporiser and substrate rotation on to ensure uniform and isotropic deposition of Parylene C on the glass substrate. Finally, the Parylene C was nicely peeled off from the glass substrate, and it was used as the flexible substrate for further processing and material characterisations. Similar methodology was adopted for deposition of ultra-thin layer of 500nm using 1g of Parylene C on top of the flexible PCB as a final step after the fabrication of the final circuit (Fig. 2).

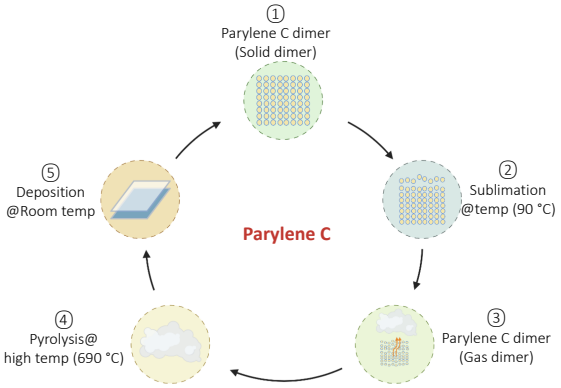


Fig. 2 | Schematic illustration of the fabrication process for thin Parylene C films, detailing substrate preparation, deposition, and final film extraction.

2.2.3 Implementation of the wireless power transfer system

For implantation in sensitive locations, such as near target organs, the device was designed for minimal invasiveness while ensuring effective operation. A single flexible polyimide PCB accommodates both the inductive power transfer coil, the tuning capacitor on the main body of the implant, and an LED array on a meandered probe, allowing it to stretch and conform to the target anatomical structure. Keysight Advanced Design Software (ADS) was used to design and simulate the geometry of the embedded inductive coil before importing the geometry to PCB design software (KiCad) for the final circuit design. An array of 4 micro-LEDs of wavelength (535 nm)[46] was used to excite the photo-synthesizable polymers with a peak absorption wavelength centred around 550 nm, as represented. The module is encapsulated with a thin, hydrophobic, and transparent layer of Parylene C of thickness (500 nm), which was used to avoid direct contact and protect it from the photosensitizer polymer.

The parallel arrangement of the LEDs enables a sufficient optical output, while the resonant circuit maximizes power reception efficiency. The device's power supply relies on a resonant inductive wireless power transfer system. The transmitter coil, connected to a signal generator and amplifier, creates a magnetic field at 6.78 MHz**.** The frequency is chosen due to its location in the Industrial, Scientific and Medical (ISM) band allowing free use; 6.78 MHz systems are widely used in biomedical wireless power transfer applications in both wearables[47] and implants[48].

2.2.4 Experimental setup for measurement of singlet oxygen generation

The generation of $^1O_2$ under PDT conditions was modelled using DPBF for the detection of singlet oxygen. The rationale is that singlet oxygen is generated from RB (photosensitizer) during illumination by the LEDs, the essence of PDT. DPBF is a fluorescent molecule that is highly reactive with singlet oxygen; the trapped singlet oxygen alters the fluorescence of DPBF, and this is detectable using suitably sensitive spectrometers.

A solution of RB and DPBF (see Section 2.2.7 for experimental design) was exposed to a continuous-wave LED with an optical power of 5 mW and 8 mW for 180 s, with 30 s intervals. The reaction vessel was a 10 mm path length

cuvette (Product No. CV10Q35, Thorlabs). After irradiating the sample, we used an in-house developed spectrophotometer setup to record the sample's absorbance spectrum. The spectrophotometer utilises a stabilised fibre-coupled light source (Product No. SLS201L/M, Thorlabs), a cuvette holder with SMA905 fibre adapter (CVH100/M), and a spectrometer (Model No. CCS200/M, Thorlabs). The light beam from the source to the cuvette holder and from the cuvette holder to the spectrometer was connected using an SMA-to-SMA multimode fibre patch cable (Product No. M92L01, Thorlabs). The cuvette holder cover (CVH100-CV, Thorlabs) was used to prevent the interaction of ambient light with the solution during absorbance measurement. The mean absorbance reading of deionised water was used as the baseline for the experiment.

2.2.5 Experimental setup for measurement of photoluminescence spectrum

The FLS1000 Photoluminescence (PL) Spectrometer (Edinburgh Instruments) was used to test our fabricated LED device. $^1O_2$ has a weak PL emission band at ~1270 nm with a natural bandwidth of ~18 nm. As the signal at 1270 nm is weak, detection of $^1O_2$ emission requires sensitive near infrared (NIR) detectors. Lifetime measurements are only possible if the detector provides sub-microsecond resolution (the radiative lifetime of $^1O_2$ is commonly 1–100 μs in solution). FLS1000 PL Spectrometer was used to characterise the PL spectrum and lifetime of $^1O_2$ in solution. Different excitation sources and detectors are compared to determine the best FLS1000 configuration for $^1O_2$ detection. The FLS1000 Spectrometer has several NIR detector options for measuring the spectrum of $^1O_2$. The three detectors compared in this technical note are: a thermoelectric (TE) cooled PMT-1400-TE, a liquid nitrogen-cooled PMT-1700-LN, and an InGaAs-1.65 analogue detector.

2.2.6 Design and testing of power circuit board

An initial testing PCB was designed to support parallel LED connections, allowing for easy adjustments to the number of LEDs, as well as control over voltage and current supplied from a DC power source. This was conducted with the PCB shown in Fig. 3(a) with the LEDs connected in parallel, each connected to a switch to allow individual LED operation. An initial small-scale prototype to test the encapsulation's effect on optical output was represented in Fig. 3(b). The optical power was quantified using the setup shown in Fig. 3(c). This consisted of an optical power meter (THOR LABS PM400) centred on top of the LEDs to allow the maximum output of the LED to be captured by the sensor, a digital multi-meter connected in series with the power supply and testing PCB to allow accurate current values supplied to the LEDs to be collected and an infrared camera to capture the temperature of the LEDs. This was measured after 5 minutes of continuous operation at the maximum respective voltage and current, allowing the LEDs to drop to room temperature between testing cycles. The distance between the light source and the sample is 1 mm apart.

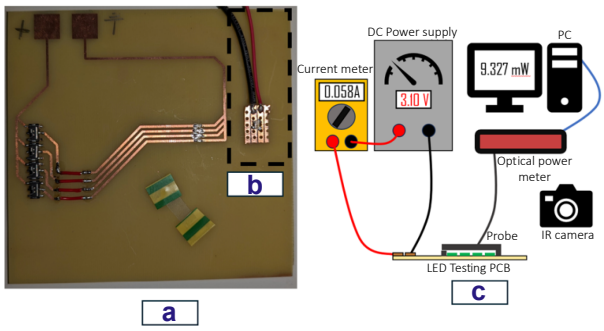


Fig. 3 | An initial testing PCB was designed to support parallel LED connections. (a) Large-scale testing PCB for individual LED quantification. (b) Initial small-scale prototype to test the encapsulation's effect on optical output. (c) The testing setup was used to quantify the LED's performance.

2.2.7 Measurement of singlet oxygen generation from RB in DMSO

The experimental setup for measurement of $^1O_2$ generation from RB in DMSO shown in Fig. 4(a, b). Figure 4(c) presents the experimental setup using a wireless 550 nm LED array for light exposure. Stock solutions of 1 mg/mL of RB (Product no. 330000, Sigma-Aldrich) in deionized water and 1 mg/mL 1,3- DPBF (Product no. 105481, Sigma-Aldrich) in DMSO (Product no. D8418, Sigma-Aldrich) were prepared. For detecting $^1O_2$ produced by the interaction of light and the photosensitizer, the stock solution of the $^1O_2$ probe was prepared by mixing further, the $^1O_2$ probe solution in photosensitizer stock solution according to the desired absorbance peak of the photosensitizer concentration.

2.2.8 Measurement of $^1O_2$ lifetime

A $^1O_2$ sample was prepared by dissolving the photosensitiser RB in DMSO to an optical density of 0.1 at 510 nm and ~0.5 at 560 nm and loaded into a quartz cuvette. The solution was saturated with air before measurements with the FLS1000 photoluminescence spectrometer (Supplementary Fig. S1) in a double excitation-double emission (DD) monochromator configuration. The spectrometer was equipped with a 450 W continuous xenon (Xe) lamp (its primary excitation source), a variable pulsed laser emitting at 510 nm (VPL-510) used for the $^1O_2$ lifetime measurement, and a visible PMT-980 and a NIR thermoelectric (TE) cooled PMT-1400 as detectors.

3 Results

3.1 Wireless-powered PDT device characterization

To ensure the implant can receive sufficient power for the LEDs, the transmission between the transmitter coil and the implanted coil was measured using a vector network

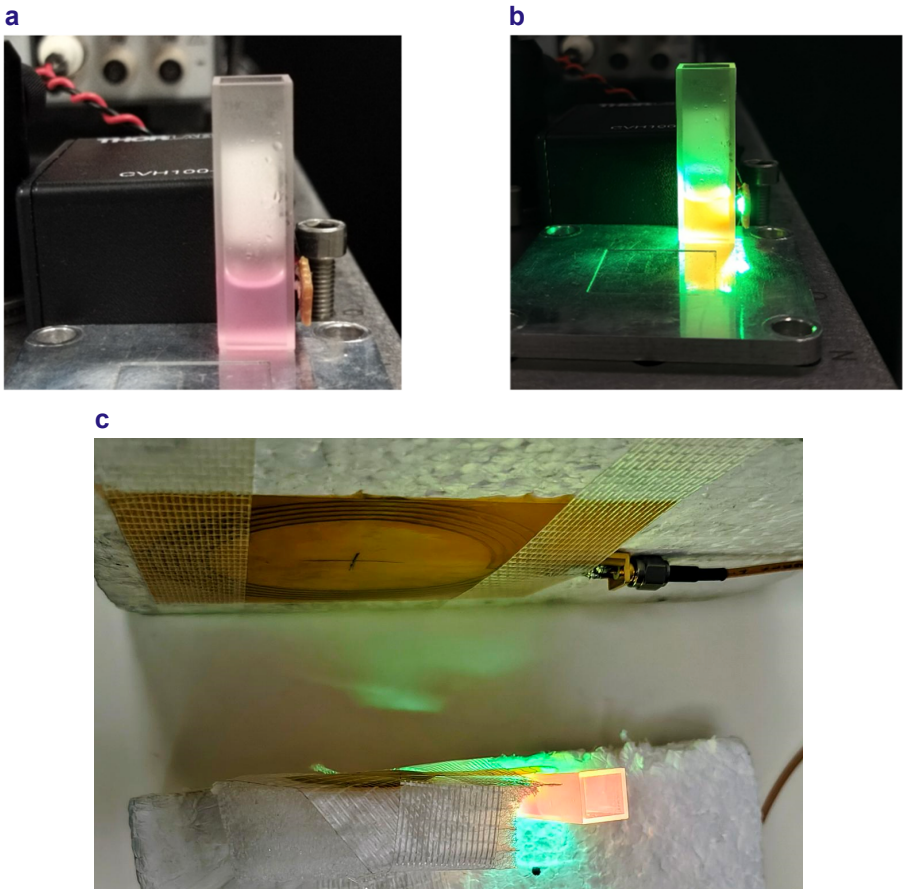


Fig. 4 | Experimental setup for illumination of RB and DPBF solution in cuvette with (a) no exposure to 550 nm light, (b) RB/DPBF exposure to 550 nm light generated by an LED array and (c) exposure with wireless 550 nm led array.

analyzer (VNA). This allows the received power to be measured under various alignment configurations, to measure how the inductive wireless power transfer (WPT) link would behave in-vivo (Fig. 5(b)). To measure the transmitted power at range, the coils were separated vertically in fixed increments measuring the transmission of the WPT link. The tests were conducted through a tissue mimicking phantom gel[49] to investigate whether this would impede the link (Fig. 5(c-i), 5(c-ii)). This was repeated for planar displacement at a 50 mm distance (Fig. 5(c-iii)) to further investigate the robustness of the power link (further alignment data presented in Supplementary Fig. S3). The drop in the transferred power follows the expected trend for inductive WPT, in either wearable or implantable use-cases, and shows the minimal interference between the magnetic field and the tissue[50]. The power loss due to the loose coupling can be compensated for by the driving amplifier, to deliver the RF power level required for the LEDs to generate the target optical power level for the drug release.

To evaluate the wireless PDT device in operation (Fig. 5(a)), the optical output of the LEDs was measured using a fast photodiode. This is presented at two different frequencies (Fig. 6(b)) to demonstrate the output more clearly, in Fig. 6(b-i) 100 kHz clearly demonstrated the half wave rectification of the voltage over the LEDs when driven with a AC input signal, however, the voltage from the photodiode clearly shows the on-off behavior of the LEDs when the polarity of the input sinusoidal voltage is matched to the polarity of the LEDs. At the wireless power frequency of 6.78 MHz (Fig. 6(b-ii)) this phenomenon can also be observed but not as clearly due to the shorter time of the input signal being above the threshold voltage of the LEDs, alongside harmonic interference from the photodiode. This is due to the capacitance of the photodiode filtering the signal received from the LEDs, lowering the signal pushing the signal to the lower limit of detection.

To investigate the heating potential of the LEDs to cause tissue damage, the device was powered using the 6.78 MHz power amplifier (GSWP50W-EVBPA) with a separation distance of 50 mm and an input power of amplifier set so that the measured optical power using the optical power meter is 5 mW. Although this is lower limit of activation of the photosensitive polymer, due to the averaging performed by the power meter the peak optical power is likely much higher than this due to the on-off behavior due to the direct AC powering. When the LEDs are operated wirelessly

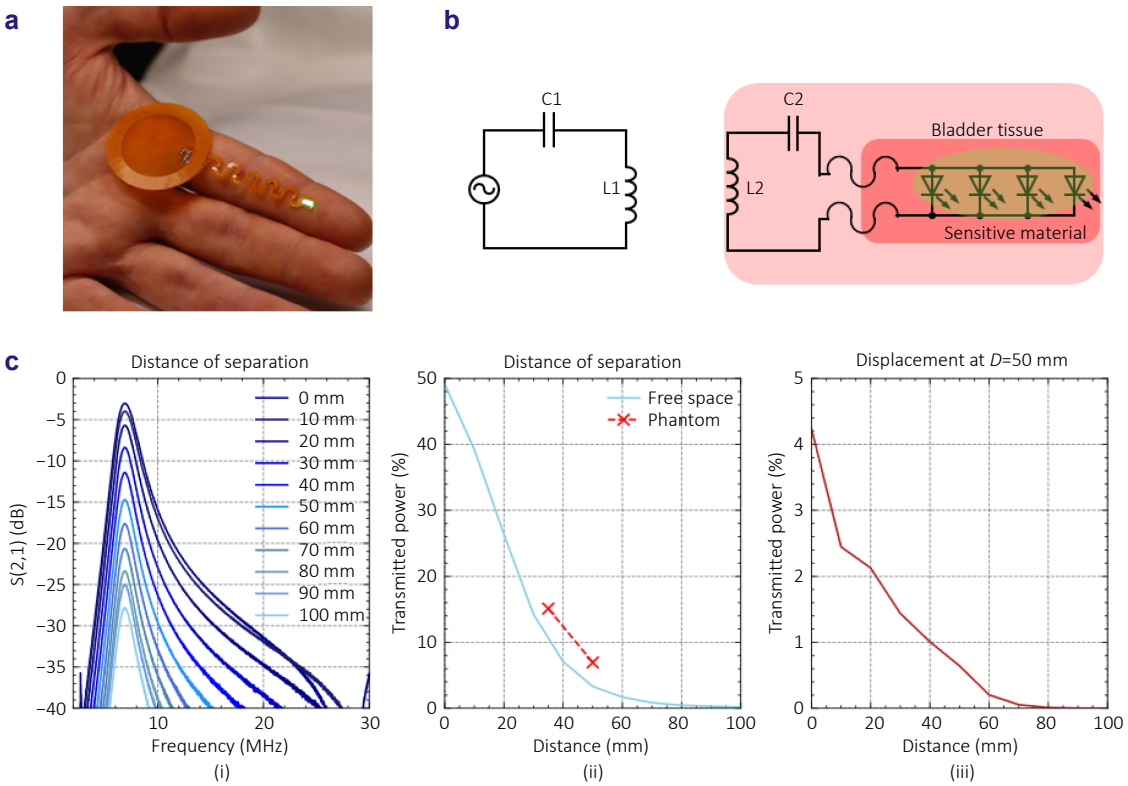


Fig. 5 | The implantable wireless power delivery characterization: (a) photograph of the fabricated device, (b) a circuit diagram of the transmitter and PDT device prototype. (c) Characterization of the device at (i) distance in the frequency domain, (ii) relative to distance at the transmission frequency and (iii) considering displacement at a separation distance of 50 mm.

(Fig. 6(c, f)) at this power output, in air and probed as shown in Fig. 6(a), they reach a steady state temperature of 80 °C in 300 seconds (Fig. 6(i)), which is above the Cumulative equivalent minutes at 43 °C (CEM_{43})[51] to cause thermal damage to surrounding tissue. However, during implantation the LEDs will be surgically implanted directly into the tumour for targeted singlet oxygen production, therefore this heat is advantageous if kept localized to the tumour and not the surrounding tissue[52,53]. In future work, we plan to couple the polymer to the device for reliable singlet oxygen production in the bladder environment and at that stage more attention can be paid to the packaging of the device including creating an enclosure for the active area of the device such as the devices discusses in ref.[54,55]. This will likely enclose the tip of the WPT device shielding the tissue from this hotspot. As such, the device was subsequently tested in several experimental setups to verify its ability to keep the generated heat localized to the tumour and not affect the healthy tissue. Tissue mimicking phantom blocks, each 50 mm-thick, were used to separate the device from the transmitter, emulating the tissue through which the power would be delivered. A thinner 10 mm slice was placed on top of the device, and a temperature probe was placed at this level. Another block 50 mm thick was placed on top of this creating an 11 cm thick block which has a large thermal mass like the abdomen (Fig. 6(d, g)). The temperature data was recorded and plotted as change in temperature to aid in comparison. Offsetting this change to a body temperature of 37 °C, we were able to deduce that the tissue heating 1 cm away from the LEDs would result in CEM_{43} of 10 min over the 300 s interval, which is below the threshold for damage (11.2 mins)[51]. To confirm that no damage was inflicted on the surrounding bladder tissue, a volume accurate model was tested using a 3D printed scaffold encased in a thin membrane placed in an insulated box (Fig. 6(e, h)). The internal volume and the outer surface of the bladder were probed and the temperature measured over time interval again resulted in an internal CEM_{43} of 2.9×10^{-3} minutes and external CEM_{43} of 1.2×10^{-3} minutes. These tests confirm that although the temperature of the LEDs locally increases to damaging levels, this heat is extremely localized to the tumour, enhancing the cytotoxic effect and the surrounding tissue remains healthy.

3.2 LED electrical and optical characterisation

To meet the optical power requirements of PDT while ensuring device miniaturization, the selected LEDs were tested to evaluate their efficiency and efficacy. The objective was to evaluate LED performance in terms of optical output,

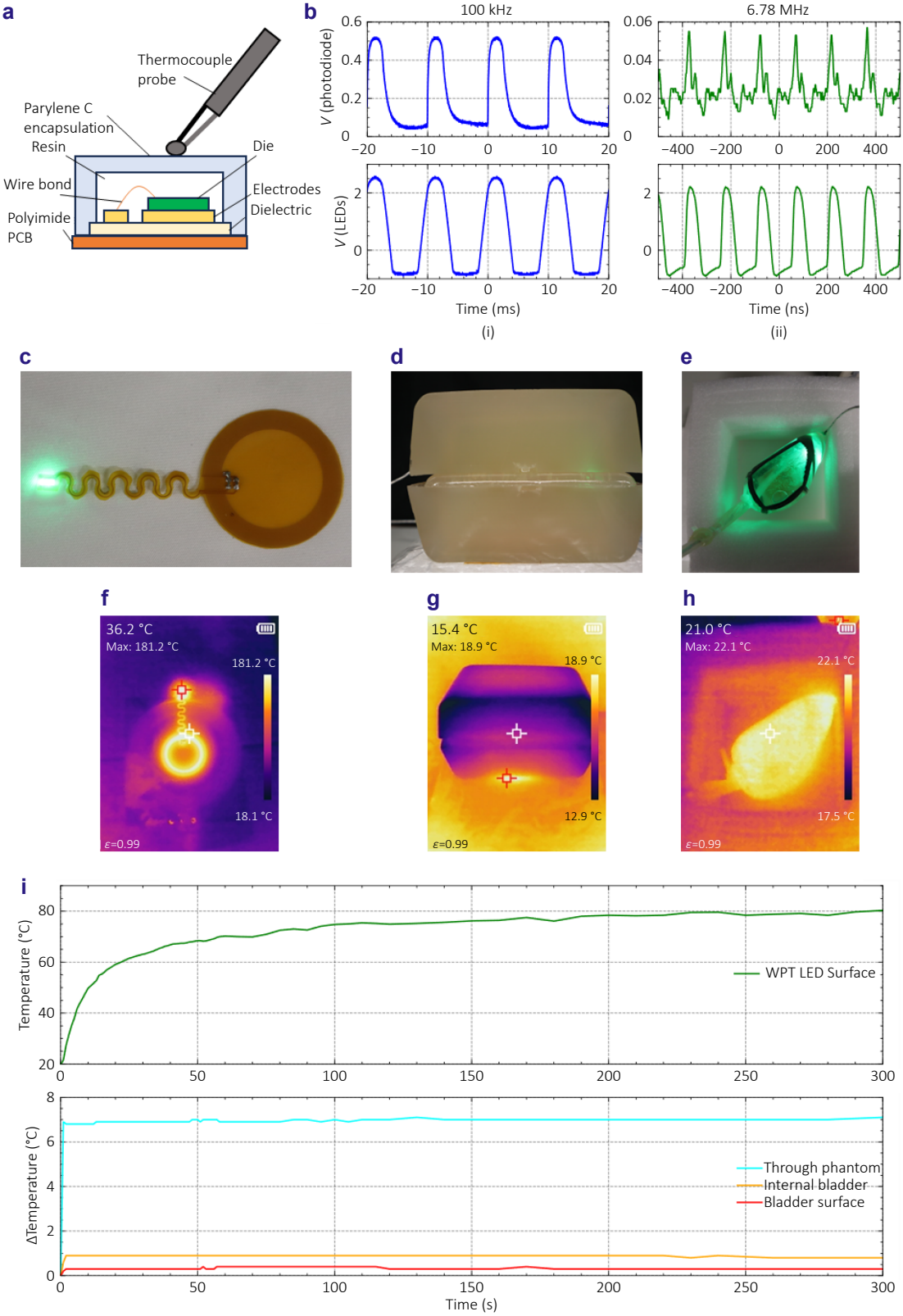


Fig. 6 | Wireless characterization of the optical output and tissue heating effect: (a) cross section of the LED including encapsulation and temperature measuring setup, (b) optical output waveform at different input frequencies, (c) the prototype device used for temperature testing with (f) IR photo, (d) the tissue mimicking phantom used for testing heat dissipation in tissue with (g) IR photo, (e) bladder phantom with equivalent volume used for heat dissipation in the implant location with (h) IR photo and (i) measured temperature of WPT LED Surface compared to the change in temperature in each of the testing setups.

current draw, and thermal behavior under various operating conditions to ensure their safety and compatibility with biological systems. An initial PCB was designed to support parallel LED connections allowing for easy modifications, including altering LED numbers, and manipulation of voltage and current supplied from a DC power source (Fig. 3). It was found that a minimum of four LEDs were required to supply the ideal output optical power intensity value of 5 – 10 mW at 550 nm (Supplementary Fig. S4). To simulate *in-vivo* conditions, the LEDs were tested with and without encapsulation in Parylene C, a biocompatible coating, to model its impact on LED performance. Results indicated that encapsulation slightly decreased the measured optical power; however, the measured value is still above the minimum to generate O^2 (Supplementary Fig. S5).

Furthermore, Fig. 7(a) shows the *I*–*V* characteristics of the LED with a positive applied sweep voltage range of 0–4 V with a compliance current of 50 mA to protect the LED. The results suggest that the current was in nanoamperes (nA) till it reached the forward voltage (V_f) of 2.3 V, and the current rose exponentially after the V_f to a maximum of 30 mA at 4 V. Next, the dynamic resistance (R_d) of the LED was calculated using the equation ($R_d=\Delta V/\Delta I$) and is obtained as 43 Ω. The sheet resistance (R_s) of the electrodes is an important parameter, and a minimal R_s is crucial to minimize the power loss, and any change might impact the overall efficiency and brightness of the LED during its operation. The R_s of the fabrication was calculated using a 4-point probe instrument (Ossila) and was obtained as 2–3 Ω/sq owing to the excellent conductivity of the gold. It should be noted that the LEDs on the gold deposited electrodes increase the required voltage to compensate for higher resistance. Furthermore, it is observed that the fabricated electrodes demonstrate a very minor change in the R_s (<0.5 Ω/sq) under different bending radii of 30°–180°. To further understand the flexibility and durability of the fabricated optoelectronic module, various bending studies were performed.

Figure 7(b) shows the optical response to both the optical power and response current from the array of 4 micro-LEDs for the applied bias voltage. The results demonstrate a linear increase in the output power with the increase in the applied bias voltage and the maximum output power dissipated from the array of LEDs is 8 mW at an applied bias voltage and current of 4 V and 60 mA, approximately. It is to be noted that each LED can illuminate a maximum power in the range of 2–2.5 mW for the same applied bias voltages, and all LEDs are connected in parallel to provide the desired power of 5 mW for the activation of the photosensitizers. Electrical tests are very important to evaluate the electrical performance of the optoelectronic module and to ensure the consistent delivery of the necessary light intensity to activate photosensitizers. In addition, to understand the behavior and electrical performance of the LED, current vs. voltage (*I*–*V*) characteristics were performed on the LED. Figure 7(c) shows the *I*–*V* characteristics of the optoelectronics

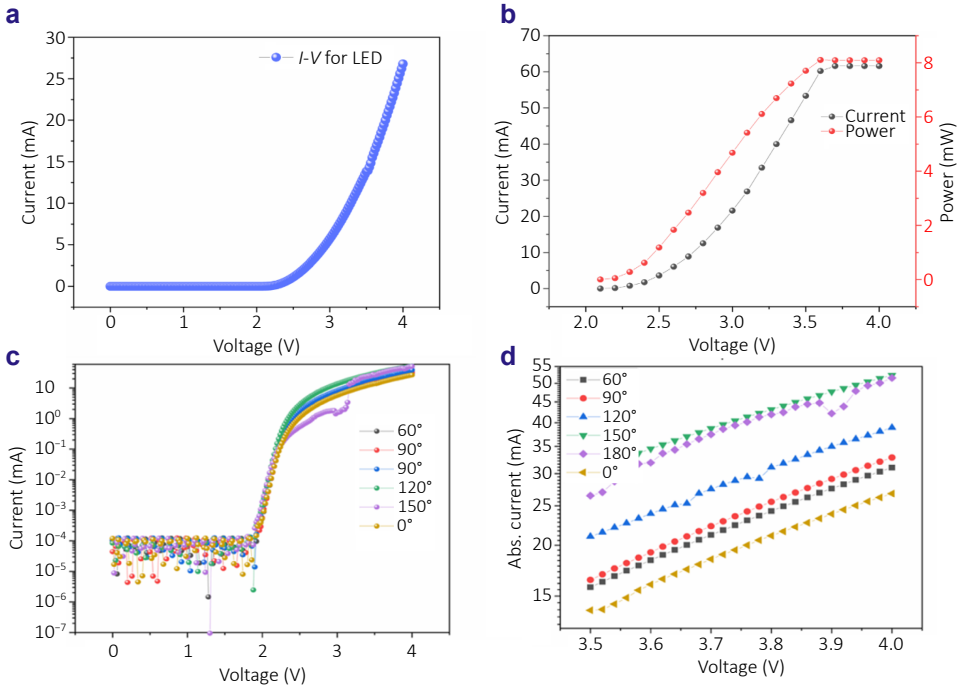


Fig. 7 | (a) Current vs voltage characteristic of the array of LEDs. (b) Output power illuminated (right) from the array of LEDs, input current (left) for the array of LEDs under an applied external voltage. (c, d) Absolute current vs. voltage characteristic under different mechanical bending radius, magnified version of the *I*–*V* characteristics under different mechanical bending.

module with LEDs under flat and at different bending radii of 60°, 90°, 120°, 150°, 180°. The results demonstrate that there is only 15% maximum relative change in the LED current as compared to the flat condition, clearly demonstrating an excellent mechanical stability under different bending conditions. Figure 7(d) shows the magnified version of the *I*–*V* characteristics for a slightly higher voltage range of 3 V to 4 V and the results demonstrate that there is 5% relative change in the current, suggesting without any major deviations in terms of the power intensity from the LED array. The primary reason for the excellent mechanical robustness of the device was mainly due to the Parylene C as a substrate with a low Young's modulus of elasticity. Further, Parylene C was used as an encapsulant to form a very good hydrophobic, biocompatible, conformable, and pinhole-free surface on the top of the module. The electrode demonstrates decent mechanical robustness under different bending cycles, and more details on the mechanical bending studies are included in the Supplementary Fig. S2.

3.3 Optical spectrum analysis

A series of initial experiments was designed to find effective concentrations of RB polymer and appropriate lengths of light irradiation for activation. The LED was operated with 2.82 V with a DC power supply (Fig. 8(a, b)). Experimental setup for illumination of RB and DPBF solution in a cuvette. The measured spectrum of the LED shows that the LED can emit light within the wavelength range of 500 nm to 540 nm, with the centre wavelength at 520 nm. Also, measured the optical power of the LED with a power meter. The LED can emit up to 12 mW.

Moreover, Figure 9 shows the absorbance spectrum of DPBF solution in DMSO after being illuminated by an 8 mW LED for 180 seconds, at 30-sec intervals. No change in the absorbance peak of DPBF was observed after illumination with the LED (Fig. 9(a)). The solution of RB and DPBF in DMSO was illuminated with LED lights of optical power 8 mW and 5 mW. Observing Fig. 9(b–d), it was noted that the solution, after being exposed to LED light for 180 seconds at 30-second intervals, showed a significant decrease in the absorbance peak of DPBF. This reduction in absorbance peak confirms the generation of singlet oxygen by LED illumination. Figure 9(d, e) shows the results of the flexible LED Parylene C flexible and biocompatible substrate with the encapsulation layer, it was noted that the solution, after being exposed to LED light for 180 seconds at 30-second intervals, showed a significant decrease in the absorbance peak of DPBF. Once again, the solution of RB and DPBF in DMSO was illuminated with LED lights of optical power 5 mW. This reduction in absorbance peak confirms the generation of singlet oxygen by LED illumination (Fig. 9(d, e)).

The intensity of $^1O_2$ luminescence is directly proportional to the efficiency of the PS. The lower the yield of $^1O_2$, the more sensitive the instrumentation required to detect it. In the case of RB in DMSO, a narrow emission band near 1270 nm from $^1O_2$ is easily identified with all three detectors but with different signal-to-noise ratios (SNR). Figure 10 shows the peak-normalised emission spectra acquired under identical conditions. In this work, S1 is refers to measurements performed on samples containing RB only, without the addition of a chemical singlet oxygen probe. The purpose of S1 was to assess the fluorescence background and to explore the feasibility of directly detecting $^1O_2$ emission under micro-LED excitation. In contrast, S2 refers to measurements performed on samples containing RB in the presence of DPBF, which acts as a chemical probe for $^1O_2$. The purpose of S2 was to enable clearer detection of $^1O_2$ emission under otherwise identical excitation conditions.

The provided micro-LEDs were attached to the cuvette and used as an excitation source for the $^1O_2$ detection, and a NIR TE-cooled PMT1400 was used as a detector. The detection of $^1O_2$ from S1 was challenging to measure, probably due to the lack of DPBF used for S2. However, a preliminary

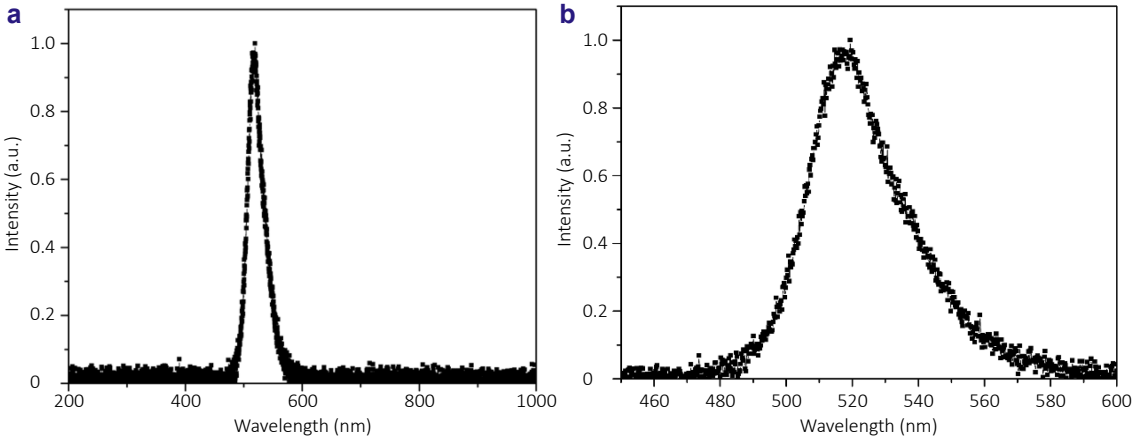


Fig. 8 | (a, b) Measured output spectrum of the LED when operated at 2.82 V using a DC power supply.

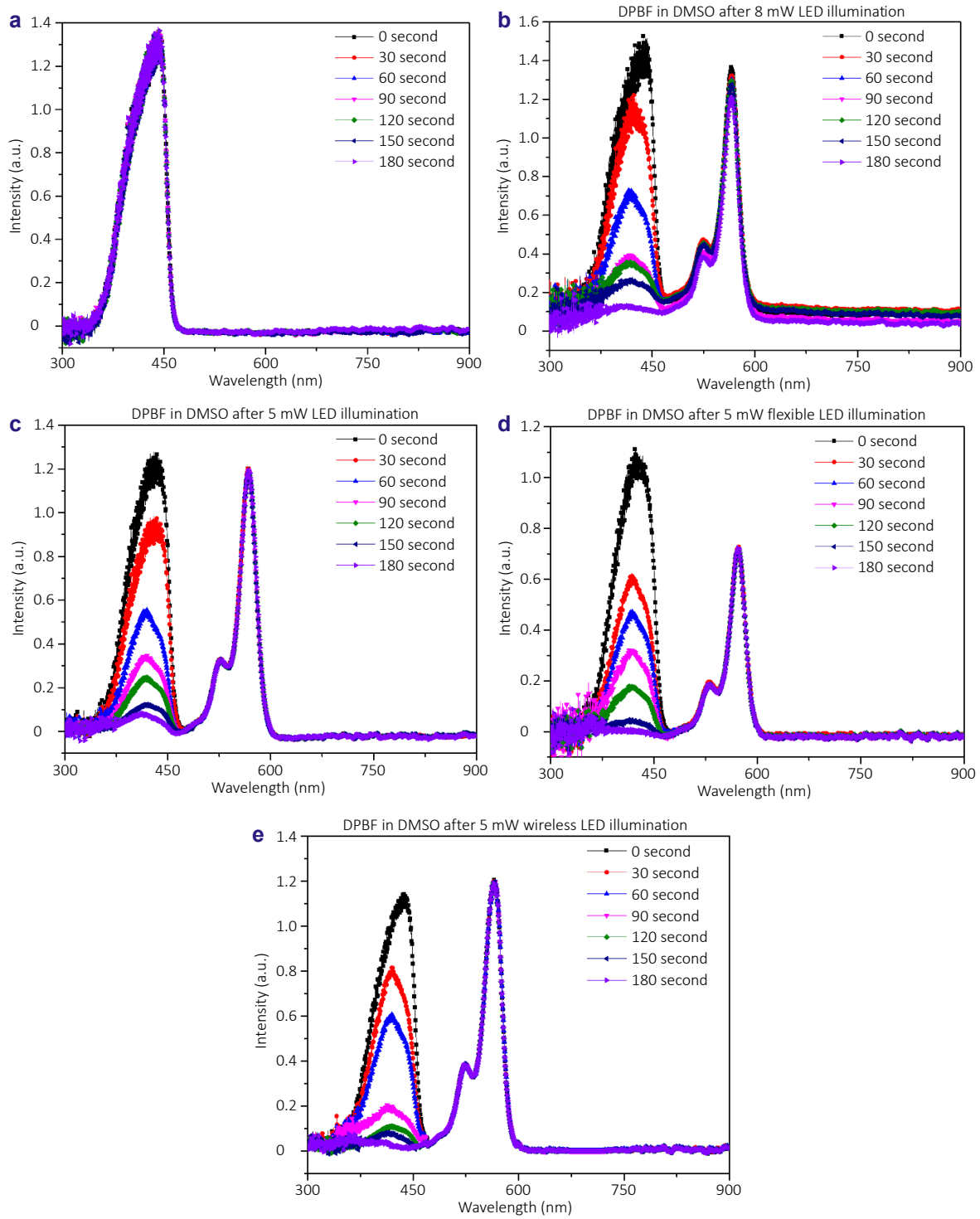


Fig. 9 | (a) The absorbance spectrum of DPBF solution in DMSO after illuminated by LED with optical power 8 mW after 0–180 second. (b) The absorbance spectrum of DPBF and RB solution in DMSO after illuminated by LED with optical power 8 mW after 0–180 seconds. The absorbance spectrum of DPBF and RB solution in DMSO after illuminated by (c) wired LED, (d) flexible led, and (e) wireless-powered, AC-driven LED system with optical power 5 mW after 0–180 seconds.

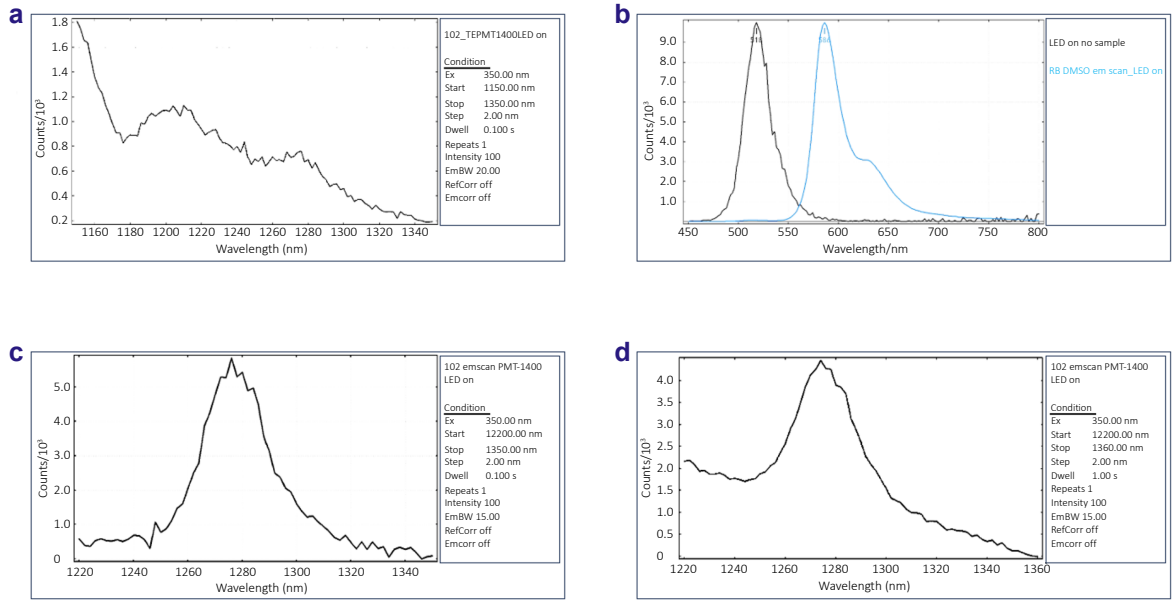


Fig. 10 | (a) S1 emission spectrum in the NIR using the provided micro-LEDs as an excitation source and a TE-cooled NIR PMT-1400. Measurement parameters: λ_{em}=1270 nm, $\Delta\lambda_{em}$=20 nm, step size=2 nm, dwell time=0.1 s. (b) Normalised emission spectrum of the micro-LEDs, in black, and fluorescence spectrum of RB, in blue. Measurement parameters for the black curve: $\Delta\lambda_{em}$=0.3 nm, step size=2 nm, dwell time=0.1 s. Measurement parameters for the blue curve: $\Delta\lambda_{em}$=0.5 nm, step size=2 nm, dwell time=0.1 s. (c) S2 $^1O_2$ emission spectrum using the provided micro-LEDs as an excitation source and a TE-cooled NIR PMT-1400. Measurement parameters: $\Delta\lambda_{em}$=15 nm, step=2 nm, dwell time=0.1 s. (d) S2 $^1O_2$ emission spectrum using the provided micro-LEDs as an excitation source and a TE-cooled NIR PMT-1400. The shoulder appearing at lower wavelengths is attributed to the RB fluorescence tail and is more prominent than that in (c). Measurement parameters: $\Delta\lambda_{em}$=15 nm, step=2 nm, dwell time=1 s.

emission spectrum (Fig. 10(a)) was acquired, potentially showing the long fluorescence tail of RB. To investigate whether any signal in that spectral region is attributed to $^1O_2$ emission, a longer measurement would be required, either by increasing the number of repeats or the dwell time. Figure 10(b) shows the normalized emission spectrum of the micro-LEDs (acquired with no sample in the sample holder, black curve) and the fluorescence spectrum of S1's RB (blue curve) using a visible PMT-980. Figure 10(c) shows the S2 $^1O_2$ emission using micro-LEDs as an excitation source and a TE-cooled PMT-1400 as a detector. Figure 10(d) shows the same but with an improved signal-to-noise ratio (SNR) as an increased dwell time was set.

The lifetime of $^1O_2$ in solution is influenced by its chemical environment, as it can undergo various reactions and non-reactive quenching simultaneously, making its lifetime challenging to predict. The most accurate approach to determining its radiative lifetime is through direct measurement using a time-resolved photoluminescence (PL) spectrometer equipped with a photon-counting detector. In this section, $^1O_2$ decay measurements were performed using a PMT-1400-TE detector within the FLS1000 system. Given that $^1O_2$ luminescence decays over a few microseconds, its lifetime was measured using multi-channel scaling (MCS). A comparison of the Xe flashlamp, VPL, and Nd:YAG lasers is presented in Supplementary Table S2. Higher pulse energies and repetition rates enable faster measurements, while wider pulses provide greater energy for quicker acquisition but at the cost of time resolution. The $^1O_2$ lifetime decay in S2 was measured using a VPL-510 (510 nm) in MCS mode, operating at 2 kHz with a 5 µs pulse width (Fig. 11(a)), 5 kHz with a 1 µs pulse width (Fig. 11(b)), and 10 kHz with a 500 ns pulse width (Fig. 11(c)). As the pulse width decreases, it becomes more distinguishable from the sample decay (Fig. 11(b, c)), which consists of two components, one of which exhibits an uprising trend. The $^1O_2$ lifetimes observed here are shorter than those reported in the literature[56,57], suggesting that the solvent in the sample may significantly quench the $^1O_2$ lifetime.

4 Discussion

The results of this study demonstrate the feasibility of using flexible wireless systems for implantable PDT in potential bladder cancer treatment applications. By integrating a biocompatible and flexible Parylene C substrate with gold microelectrodes and a micro-LED array, the proposed system successfully delivers controlled optical power while maintaining mechanical robustness under various bending conditions. The system's ability to generate $^1O_2$ using RB in DMSO further confirms its potential for effective PDT applications. The generated optical power of DC-driven and wireless-powered, AC-driven, LEDs was found to be capable of generating $^1O_2$ under phantom-based testing, when

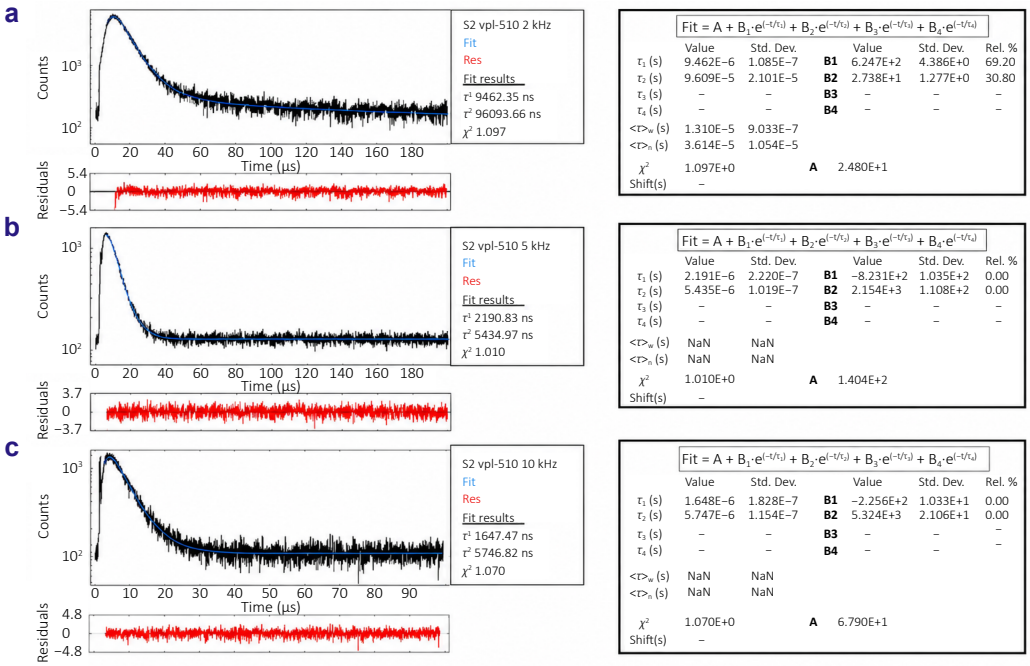


Fig. 11 | (a) Lifetime decay of S2 $^1O_2$ using a VPL-510 at 2 kHz with a 5 μs pulse width. Measurement parameters: λ_{ex}=510 nm, λ_{em}=1270 nm, $\Delta\lambda_{em}$=20 nm, # of channels=2k, step=0.1 μs. (b) Lifetime decay of S2 $^1O_2$ using a VPL-510 at 5 kHz with a 1 μs pulse width. Measurement parameters: λ_{ex}=510 nm, λ_{em}=1270 nm, $\Delta\lambda_{em}$=20 nm, # of channels=2k, step=0.1 μs. (c) Lifetime decay of S2 $^1O_2$ using a VPL-510 at 10 kHz with a 500 ns pulse width. Measurement parameters: λ_{ex}=510 nm, λ_{em}=1270 nm, $\Delta\lambda_{em}$=20 nm, # of channels=2k, step=0.1 μs.

driven by a 6.78 MHz within previous safety limits.

Traditional PDT systems rely on external laser light sources delivered through fibre optics or endoscopic systems, which pose several limitations, including limited light penetration, inconvenient setup, and the need for repeated invasive procedures[58]. Moreover, these approaches require bulky laser systems, making them unsuitable for continuous or localized therapy. In contrast, the proposed wireless, implantable PDT microsystem overcomes these limitations by providing continuous, localized light delivery, eliminating the need for frequent interventions[59]. Compared to other implantable photonic systems, such as tissue-adhesive wireless optoelectronic devices, our system offers significant advantages in flexibility, miniaturization, and fabrication scalability.

Most conventional cleanroom-based microfabrication techniques for PDT devices are time-consuming, costly, and involve toxic chemicals, which can compromise biocompatibility. In contrast, the ultrafast laser ablation-based fabrication introduced in this study is cost-effective, scalable, and adaptable to various biocompatible materials. This fabrication approach enhances design flexibility, allowing for precise micro-patterning with high resolution, which is crucial for miniaturized implantable devices. The optoelectronic performance of the fabricated LED system was validated through electrical and optical characterizations. The IV characteristics demonstrated stable current flow with minimal power loss, ensuring efficient energy conversion. The device also showed excellent mechanical robustness under bending angles ranging from 30° to 180°. This confirms the feasibility of integrating the device into dynamic biological environments, such as the bladder, without significant degradation in performance. A critical aspect of PDT efficacy is the ability of the system to generate ROS, particularly $^1O_2$, which induces cancer cell apoptosis[60]. The reduction in the absorbance peak of DPBF after LED exposure confirms successful $^1O_2$ generation. Further photoluminescence (PL) studies using the FLS1000 spectrometer provided direct evidence of $^1O_2$ emission at 1270 nm, a key indicator of PDT efficiency. The lifetime decay measurements suggested that $^1O_2$ persisted long enough for effective photodynamic interactions, validating the therapeutic relevance of the device. While the results are promising, several factors must be considered for clinical translation. One major challenge is WPT efficiency. The current system operates at 6.78 MHz, utilizing an inductive coil receiver for energy harvesting. Although sufficient for LED activation, optimizing power rectification will be crucial for stable and prolonged operation *in-vivo*. Additionally, thermal management is a key consideration, as excessive heat generation from the micro-LEDs could cause tissue damage[61]. Future work will explore efficient heat dissipation strategies, such as improved encapsulation materials or thermal regulation circuits. Another consideration is long-term biocompatibility.

While Parylene C is known for its excellent biostability and hydrophobicity, *in-vivo* studies will be necessary to assess potential immune responses or biofouling effects. The next phase of research will involve *in-vitro* biocompatibility testing, followed by *in-vivo* implantation studies to evaluate the long-term stability and therapeutic effectiveness of the device. Additionally, the effectiveness of benzothiadiazole-based polymers as an alternative photosensitizer will be tested to determine if they offer higher efficiency, longer excitation wavelengths, or reduced toxicity compared to RB. Expanding the range of photosensitizers will make the system more adaptable to different cancer types beyond bladder cancer.

The successful development of a wireless, implantable PDT system represents a paradigm shift in cancer treatment. Unlike traditional PDT, which is limited by light accessibility issues, this implantable solution allows for deep-seated tumor treatment with precise spatial and temporal light control. The ability to combine PDT with other therapeutic modalities such as chemotherapy, immunotherapy, or gene therapy could significantly improve treatment outcomes while minimizing systemic side effects. By addressing the technical challenges outlined above, the proposed laser-ablated microsystem could serve as a clinically viable, minimally invasive alternative for localized, recurrent bladder cancer treatment. Future research will refine its power management, biocompatibility, and therapeutic efficacy, paving the way for next-generation implantable medical devices tailored for precision oncology applications. Subsequently, our strategy could improve treatment outcomes and potentially increase patients' post-therapy comfort and satisfaction by reducing debilitating Adverse Events (AEs) associated with high dose drugs and high irradiance PDT. These findings suggest the potential suitability of the system for in vivo use; however, this has not yet been directly validated. This method may have potential for future therapeutic application, although additional studies are required to evaluate its safety, efficacy, and translational feasibility. Also, future work will focus on systematic in vivo validation, optimisation of operating parameters, and assessment of long-term biocompatibility to support potential clinical translation.

5 Conclusion

In this study, we successfully designed, fabricated, and characterized a flexible wireless microsystem for implantable PDT. The experimental results demonstrated the optical, electrical, and mechanical reliability of the system. Electrical characterizations confirmed a stable current-voltage relationship, while bending tests showed that the device maintains over 85% of its performance even under significant mechanical deformation. This flexibility indicates that the device can adapt to the dynamic environment of the bladder, reducing mechanical stress and potential device failure.

A critical aspect of PDT efficacy is the generation of $^1O_2$, which induces cancer cell apoptosis. The *in-vitro* PL measurements confirmed successful $^1O_2$ generation, with a reduction in DPBF absorbance following LED exposure, indicating efficient photodynamic activation. The $^1O_2$ emission spectrum at 1270 nm was validated using an FLS1000 spectrometer, demonstrating that the system effectively triggers photochemical reactions necessary for PDT. Furthermore, we have evidenced the performance of a flexible, biocompatible, and implantable optoelectronic system fabricated using a laser ablation-based technique on a Parylene C substrate with gold patterned electrodes illustrates a promising advantage in the field of PDT. The fabricated system demonstrates good optoelectronic performance with the maximum light illumination intensity of greater than 16 mW from 4 LEDs, excellent mechanical robustness under different bending radius varying from 30° to 180°, and biocompatibility specifically targeted for the treatment modalities. The system demonstrates excellent mechanical flexibility. $^1O_2$ emission and lifetime were successfully measured using an FLS1000-DD Photoluminescence Spectrometer.

The single-single (SS) configuration would be equally adequate for the measurements shown in this paper, and it is recommended for $^1O_2$ detection with all the parameters that was measured. The reduction in absorbance peak of DPBF confirms the generation of $^1O_2$ by LED illumination. The proposed configuration is as follows, FLS1000-SS monochromators, PMT-900 since the fluorescence of the samples was within the detector's range (or PMT-980), TE-cooled NIR PMT-1400 for $^1O_2$ measurements, N-J01 standard cuvette holder, MCS electronics, VPL-510 laser diode. A fabrication approach employing rapid prototyping and ultra-fast laser ablation-based fabrication was also explored, which ensures high-resolution patterning, scalability, and compatibility with flexible, biocompatible materials, making it a promising alternative to conventional cleanroom-based microfabrication methods.

This research advances the development of a compact, wirelessly powered implantable device for PDT, optimized for *in-vivo* use through careful LED selection, effective wireless power transfer, and a flexible, biocompatible design. Overall, this study evidence that a flexible potentially biocompatible device can be fabricated in a cost-effective manner. Our results evidence the potential of a new emergent technology that addresses the limitations of PDT as a potential future mono or combination therapy as to enhance the curative efficiency of cancer treatment without the need for repeated invasive interventions. Although, the proposed system shows promise for in vivo therapeutic applications, but further validation in relevant biological models is required. It should be noted that the current study is limited to in vitro, simulated and controlled conditions, and comprehensive in vivo studies will be necessary to fully assess biological performance, safety, and therapeutic

efficacy. Furthermore, this study establishes a proof-of-concept platform, providing a foundation for future investigations toward clinical translation.

6 Clinical implications & future directions

The advances presented in our research demonstrating the performance of a wirelessly powered, fully implantable PDT system represent a significant advancement in cancer treatment, offering a continuous, localized light source for deep-seated tumors. Unlike traditional PDT, which relies on external laser systems and endoscopic fiber optics, this system eliminates the need for repeated invasive procedures, improving patient comfort and treatment accessibility. Moreover, by integrating wireless power transfer (WPT), the device can be remotely activated without requiring physical connections, enhancing clinical usability.

Future research will focus on several open questions which must be addressed before clinical translation. For example, optimizing power rectification will be essential to improve energy efficiency and long-term stability. Additionally, thermal management strategies need to be explored to prevent heat accumulation that could damage surrounding tissues. Furthermore, work will focus on *in-vitro* biocompatibility testing, followed by *in-vivo* animal studies to evaluate long-term performance and safety.

The potential of benzothiadiazole-based polymers as alternative photosensitizers will also be investigated to determine their suitability for broader cancer applications. Future optimization of the technology will also prioritize further miniaturization of the device while maintaining high optical output. New capabilities of this implantable transponder will also be explored, such as the integration of real-time monitoring and data logging capabilities, along with wireless communication modules, towards enabling personalized, adaptive therapy where treatment parameters are dynamically adjusted based on patient-specific responses.

Also, future refinements to this device will focus on multiple aspects including optimizing power rectification for improved performance and enabling the device to record and communicate, in real-time, key parameters such as exposure period, and number of instances it was used, which will be key in the assessment of the patient's case. This will require re-designing the device to incorporate key components such as local storage (flash memory), wireless communication, e.g., Wi-Fi or LoRa, and power management modules. The encapsulated devices will undergo *in vitro* and *in vivo* testing to validate their potential biocompatibility and evaluate any of the target toxicities of the device during active PDT at cellular or tissue levels. Moreover, biological assessments such as evaluating ROS production, cytotoxicity, apoptosis-related markers, and appropriate dark toxicity controls are currently underway in our laboratory for future paper. Further testing will establish the physical penetration range of the light within tissues and/or organoids.

The efficacy of Benzothiadiazole-based polymers will be tested against photosensitizers already in clinical use to evaluate their use in a range of cancer types and to evaluate the effectiveness of this approach. Finally, this innovative approach demonstrates that PDT treatment is potentially feasible using implanted devices, with local administration of photosensitizer polymers. Such devices could provide PDT treatment to the tumour site for the duration of clinical management resulting in tumour control at the local site.

Furthermore, a fully stretchable and conformable substrate materials will be used for the fabrication of the fully implantable PDT microsystem, and a miniatured electrode system will be proposed with a stacked layer with a very dielectric separation layer. Ultimately, this research lays out the groundwork for next-generation implantable medical microsystems, capable of providing precise, non-invasive, and effective cancer therapy. By addressing key technical challenges, this system has the potential to become a clinically viable, widely adaptable solution for personalized, minimally invasive oncology treatments.

References

1. Sung H, Ferlay J, Siegel RL et al. Global cancer statistics 2020: GLOBOCAN estimates of incidence and mortality worldwide for 36 cancers in 185 countries. *CA Cancer J Clin* **71**, 209–249 (2021).
2. Society TAC. The Global Cancer Burden | American Cancer Society. Cancer. org [Internet]. [cited 2025 Feb 3]. Available from: https://www.cancer.org/about-us/our-global-health-work/global-cancer-burden.html.
3. Rindi G, Klimstra DS, Abedi-Ardekani B et al. A common classification framework for neuroendocrine neoplasms: an International Agency for Research on Cancer (IARC) and World Health Organization (WHO) expert consensus proposal. *Mod Pathol* **31**, 1770–1786 (2018).
4. Marino P, Mininni M, Deiana G et al. Healthy lifestyle and cancer risk: modifiable risk factors to prevent cancer. *Nutrients* **16**, 800 (2024).
5. Gallegos ER, Deleón Rodríguez I, Martínez Guzmán LA et al. *In vitro* study of biosynthesis of protoporphyrin IX induced by δ-aminolevulinic acid in normal and cancerous cells of the human cervix. *Arch Med Res* **30**, 163–170 (1999).
6. Bentzen SM. Preventing or reducing late side effects of radiation therapy: radiobiology meets molecular pathology. *Nat Rev Cancer* **6**, 702–713 (2006).
7. Qiao J, Liu ZD, Fu YX. Adapting conventional cancer treatment for immunotherapy. *J Mol Med* **94**, 489–495 (2016).
8. Keating NL, Beth Landrum M, Arora NK et al. Cancer patients' roles in treatment decisions: do characteristics of the decision influence roles. *J Clin Oncol* **28**, 4364–4370 (2010).
9. Kubrak T, Karakuła M, Czop M et al. Advances in management of bladder cancer—The role of photodynamic therapy. *Molecules* **27**, 731 (2022).
10. Lopez-Beltran A, Cookson MS, Guercio BJ et al. Advances in diagnosis and treatment of bladder cancer. *BMJ* **384**, e076743 (2024).
11. Nakatani S, Ida M, Wang XY et al. Oral 5-aminolevulinic acid administration prior to transurethral resection of bladder tumor causes intraoperative hypotension: propensity score analysis.

Photodiagnosis Photodyn Ther **34**, 102342 (2021).
12. Kirkali Z, Chan T, Manoharan M et al. Bladder cancer: epidemiology, staging and grading, and diagnosis. *Urology* **66**, 4–34 (2005).
13. Kudinova NV, Berezov TT. Photodynamic therapy of cancer: search for ideal photosensitizer. *Biochem Mosc Suppl B Biomed Chem* **4**, 95–103 (2010).
14. Ou-Yang Y, Zheng YW, Mills KE. Photodynamic therapy for skin carcinomas: a systematic review and meta-analysis. *Front Med* **10**, 1089361 (2023).
15. Fukuhara H, Yamamoto S, Karashima T et al. Photodynamic diagnosis and therapy for urothelial carcinoma and prostate cancer: new imaging technology and therapy. *Int J Clin Oncol* **26**, 18–25 (2021).
16. Li HT, Long GW, Tian J. Efficacy and safety of photodynamic therapy for non-muscle-invasive bladder cancer: a systematic review and meta-analysis. *Front Oncol* **13**, 1255632 (2023).
17. Sun BW, Bte Rahmat JN, Zhang Y. Advanced techniques for performing photodynamic therapy in deep-seated tissues. *Biomaterials* **291**, 121875 (2022).
18. Bansal A, Yang FY, Xi T et al. In vivo wireless photonic photodynamic therapy. *Proc Natl Acad Sci U S A* **115**, 1469–1474 (2018).
19. Chilakamarthi U, Giribabu L. Photodynamic therapy: past, present and future. *Chem Rec* **17**, 775–802 (2017).
20. Kim MM, Darafsheh A. Light sources and dosimetry techniques for photodynamic therapy. *Photochem Photobiol* **96**, 280–294 (2020).
21. Choi J, Lee IS, Lee JS et al. Implantable micro-scale LED device guided photodynamic therapy to potentiate antitumor immunity with mild visible light. *Biomater Res* **26**, 56 (2022).
22. Yamagishi K, Kirino I, Takahashi I et al. Tissue-adhesive wirelessly powered optoelectronic device for metronomic photodynamic cancer therapy. *Nat Biomed Eng* **3**, 27–36 (2019).
23. Thiruppathi J, Vijayan V, Park IK et al. Enhancing cancer immunotherapy with photodynamic therapy and nanoparticle: making tumor microenvironment hotter to make immunotherapeutic work better. *Front Immunol* **15**, 1375767 (2024).
24. Hoseini-Ghahfarokhi M, Olofinsan KA, Sarbadhikary P et al. Editorial: combination of photodynamic therapy and immunotherapy to overcome cancer resistance. *Front Immunol* **17**, 1833324 (2026).
25. Korbelik M, Banáth J, Saw KM et al. Calreticulin as cancer treatment adjuvant: combination with photodynamic therapy and photodynamic therapy-generated vaccines. *Front Oncol* **5**, 15 (2015).
26. Algorri JF, Ochoa M, Roldán-Varona P et al. Light technology for efficient and effective photodynamic therapy: a critical review. *Cancers* **13**, 3484 (2021).
27. Attili SK, Lesar A, McNeill A et al. An open pilot study of ambulatory photodynamic therapy using a wearable low-irradiance organic light-emitting diode light source in the treatment of nonmelanoma skin cancer. *Br J Dermatol* **161**, 170–173 (2009).
28. Kim SJ, Kim HD, Kim KH et al. Fabrication of wide-bandgap transparent electrodes by using conductive filaments: performance breakthrough in vertical-type GaN LED. *Sci Rep* **4**, 5827 (2014).
29. Dudzik T, Domański I, Makuch S. The impact of photodynamic therapy on immune system in cancer – an update. *Front Immunol* **15**, 1335920 (2024).
30. Qasaimeh MA, Sokhanvar S, Dargahi J et al. PVDF-based microfabricated tactile sensor for minimally invasive surgery. *J Microelectromech Syst* **18**, 195–207 (2009).
31. Dobruch J, Oszczudłowski M. Bladder cancer: current challenges and future directions. *Medicina* **57**, 749 (2021).
32. Ahangar M, Mahjoubi F, Mowla SJ. Bladder cancer biomarkers: current approaches and future directions. *Front Oncol* **14**, 1453278 (2024).
33. Mohanty SK, Lobo A, Mishra SK et al. Precision medicine in bladder cancer: present challenges and future directions. *J Pers Med* **13**, 756 (2023).
34. Kochergin M, Fahmy O, Asimakopoulos A et al. Photodynamic therapy: current trends and potential future role in the treatment of bladder cancer. *Int J Mol Sci* **25**, 960 (2024).
35. Geng CY, Li CY, Li W et al. A simple fabricated microfluidic chip for urine sample-based bladder cancer detection. *J Micromech Microeng* **28**, 115011 (2018).
36. Yang YY, Wu MZ, Wegener AJ et al. Preparation and use of wireless reprogrammable multilateral optogenetic devices for behavioral neuroscience. *Nat Protoc* **17**, 1073–1096 (2022).
37. Scholten K, Meng E. Materials for microfabricated implantable devices: a review. *Lab Chip* **15**, 4256–4272 (2015).
38. Chen K, Ren JY, Chen CY et al. Safety and effectiveness evaluation of flexible electronic materials for next generation wearable and implantable medical devices. *Nano Today* **35**, 100939 (2020).
39. Karlapudi MC, Vahdani M, Bandari SM et al. A comparative study on the effects of spray coating methods and substrates on polyurethane/carbon nanofiber sensors. *Sensors* **23**, 3245 (2023).
40. Chiulan I, Frone AN, Brandabur C et al. Recent advances in 3D printing of aliphatic polyesters. *Bioengineering* **5**, 2 (2018).
41. Chen JM, Fan TJ, Xie ZJ et al. Advances in nanomaterials for photodynamic therapy applications: status and challenges. *Biomaterials* **237**, 119827 (2020).
42. Thanjavur N, Bugude L, Kim YJ. Integration of functional materials in photonic and optoelectronic technologies for advanced medical diagnostics. *Biosensors* **15**, 38 (2025).
43. Karimi K, Fardoost A, Mhatre N et al. A thorough review of emerging technologies in micro- and nanochannel fabrication: limitations, applications, and comparison. *Micromachines* **15**, 1274 (2024).
44. Yamada A, Niikura F, Ikuta K. A three-dimensional microfabrication system for biodegradable polymers with high resolution and biocompatibility. *J Micromech Microeng* **18**, 025035 (2008).
45. Sun BW, Bte Rahmat JN, Kim HJ et al. Wirelessly activated nanotherapeutics for in vivo programmable photodynamic-chemotherapy of orthotopic bladder cancer. *Adv Sci* **9**, 2200731 (2022).
46. ams-OSRAM AG. LT Q39E datasheet [Internet]. [cited 2026 Mar 31]. Available from: https://look.ams-osram.com/m/494f1cf6b7ac7c03/original/LT-Q39E.pdf.
47. Ullah I, Wagih M, Sun YX et al. Wirelessly powered drug-free and anti-infective smart bandage for chronic wound care. *IEEE Trans Biomed Circuits Syst* **17**, 900–915 (2023).
48. Shah IA, Basir A, Cho Y et al. Safety analysis of medical implants in the human head exposed to a wireless power transfer system. *IEEE Trans Electromagn Compat* **64**, 640–649 (2022).
49. Bruce N, Wagih M. Simulated in vivo implantable antenna measurements in gel phantoms and human subjects: channel gain, directivity, and received signal strength indicator [Bioelectromagnetics]. *IEEE Antennas Propag Mag* **68**, 62–115 (2026).
50. Wagih M, Komolafe A, Ullah I et al. A wearable all-printed textile-based 6.78 MHz 15 W-output wireless power transfer system and its screen-printed joule heater application. *IEEE Trans Ind Electron* **71**, 3741–3750 (2024).
51. Yarmolenko PS, Moon EJ, Landon C et al. Thresholds for thermal damage to normal tissues: an update. *Int J Hyperthermia* **27**, 320–343 (2011).
52. Al-Zu'bi M, Mohan A. Modelling of combination therapy using implantable anticancer drug delivery with thermal ablation in solid tumor. *Sci Rep* **10**, 19366 (2020).
53. Portosi V, Loconsole AM, Valori M et al. Low-cost mini-invasive microwave needle applicator for cancer thermal ablation: feasibility investigation. *IEEE Sens J* **21**, 14027–14034 (2021).
54. Koo J, Kim SB, Choi YS et al. Wirelessly controlled, bioresorbable drug delivery device with active valves that exploit electrochemically triggered crevice corrosion. *Sci Adv* **6**, eabb1093 (2020).
55. Krawczyk K, Xue S, Buchmann P et al. Electrogenetic cellular insulin release for real-time glycemic control in type 1 diabetic mice.

Science **368**, 993–1001 (2020).
56. Moskalensky AE, Karogodina TY, Vorobev AY et al. Singlet oxygen luminescence detector based on low-cost InGaAs avalanche photodiode. *HardwareX* **10**, e00224 (2021).
57. https://www.edinst.com/singlet-oxygen-detection-2/ - Google Search [Internet]. [cited 2025 Mar 11]. Available from: https://www.google.com/search?q=%3A+https%3A%2F%2Fwww.edinst.com%2Fsinglet-oxygen-detection-2%2F.
58. Mallidi S, Anbil S, Bulin AL et al. Beyond the barriers of light penetration: strategies, perspectives and possibilities for photodynamic therapy. *Theranostics* **6**, 2458–2487 (2016).
59. Kim A, Zhou JW, Samaddar S et al. An implantable ultrasonically-powered micro-light-source (μLight) for photodynamic therapy. *Sci Rep* **9**, 1395 (2019).
60. Ming L, Cheng K, Chen Y et al. Enhancement of tumor lethality of ROS in photodynamic therapy. *Cancer Med* **10**, 257–268 (2021).
61. Ji YP, Liu CZ, Li JW et al. A photothermal modelling approach for micro-LED arrays in wireless optogenetics. *Int J Distrib Sens Netw* **2024**, 5562848 (2024).

Acknowledgements

We acknowledge the funding support from the Engineering and Physical Sciences Research Council (EPSRC) via the PATIENT project (EP/X017516/1). We would like to thank Mr. Hossein Parvizi for his help and support with photo preparation throughout the project.
This work is supported by Engineering and Physical Sciences Research Council (EPSRC) via the PATIENT project (EP/X017516/1). The research within this paper is a recipient of the Institution of Engineering and Technology (IET) Healthcare Technology of the Year Award 2024.

Author contributions

Rolan Mansour: – Writing – original draft, Software, Methodology, Formal analysis. Bhavani Yalagala: – Writing – original draft, Software, Methodology, Formal analysis. Vikas Vikas: – Writing – original draft, Software, Methodology, Formal analysis. Nikolas Bruce: – Writing – original draft, Software, Methodology, Formal analysis. Fawziye Tarhini: – Writing – original draft, Software, Methodology, Formal analysis. Georgios N. Arvanitakis: – Writing – review & editing, Writing – original draft. Jamie Blanche: – Writing – review & editing. Ahmad Taha: Writing – review & editing, Writing – original draft. Jonathan Copper: – Writing – review & editing. Muhammad Imran: – Writing – review & editing. Karin Williams: – Writing – review & editing, Writing – original draft. Karin Oien: – Writing – review & editing. Mahmoud Wagih: – Writing – review & editing. Hadi Heidari: – Writing – review & editing. Robert Hadfield: - Writing – review & editing. David Flynn: – Conceptualisation, Ideation, Methodology, Review, Editing, Validation, Resources, and Supervision.

Competing interests

The authors declare that they have no known competing financial interests or personal relationships that could have appeared to influence the work reported in this paper.

Data availability

Data available on request from the authors: “Data supporting this study are included within the article” The data that support the findings of this study are available from the corresponding author, [Rolan Mansour], upon reasonable request.

Abbreviations

PC - Parylene C; LED - light emitting diode; RB - Rose Bengal; DMSO - Dimethyl sulfoxide; DPBF-1,3 - Diphenylisobenzofuran; PDT - Photodynamic therapy; NIR - Near Infrared; Ti/Au – Titanium/Gold; PL - Photoluminescence; IPA - Isopropyl Alcohol; PCB - Printed Circuit Board; 1O2 - singlet oxygen; WPT- wireless power transfer, CEM43- Cumulative equivalent minutes at 43 °C.

Open Access This article is licensed under a Creative Commons Attribution 4.0 International License, which permits use, sharing, adaptation, distribution and reproduction in any medium or format, as long as you give appropriate credit to the original author(s) and the source, provide a link to the Creative Commons license, and indicate if changes were made. To view a copy of this license, visit http://creativecommons.org/licenses/by/4.0/
©The Author(s) 2026.
Published by Editorial Office of *Opto-Electronic Advance*, Institute of Optics and Electronics, Chinese Academy of Sciences.

Opto-Electronic Journals Group
www.oejournal.org
Scan for Article PDF